A Data Driven Approach to Identify Optimal Thermal Parameters for Finite Element Analysis of Electric-Assisted Deformation Processes

Jai Tiwari[1] · Bashista Kumar Mahanta[2] · Hariharan Krishnaswamy[1] · Sivasrinivasu Devadula[1] ·
Murugaiyan Amirthalingam[3]

Abstract

Application of electric current pulses while deforming a material, commonly referred to as electric-assisted forming (EAF), is known to have desirable effects over its formability. In the finite element simulation of this electric-assisted deformation, the time-temperature profile is obtained by providing various temperature dependent thermo-physical properties of the material. Out of all the required properties for such analysis, effective heat transfer coefficient and Joule heat fraction are sensitive to the microstructure of the material, geometry of the specimen and the ambient conditions. Generally, these coefficients are identified by iterative FE simulations. A clear methodology to estimate these parameters has not been established yet. In the present work, a procedure is developed using a genetically evolved meta-model of the time-temperature profile, which is experimentally obtained from the pulsed current assisted uniaxial tension and compression tests. For this purpose, various multi-objective optimization techniques such as BioGP, EvoNN and cRVEA have been utilized to estimate the temperature profile in each case. It is shown that the tri-objective optimization procedure predicts the experimental temperature profile with greater accuracy (within ± 5%) and is best suited to obtain the thermal modelling parameters of electric-assisted deformation, than other optimization techniques used in this work.

1 Introduction

Electric-assisted forming (EAF) is a modern manufacturing method in which application of electric current pulses favourably assist the deformation process [1, 2]. Reduction in the flow stress and enhancement of the ductility are observed with electric-assisted deformation [3, 4]. Other advantages of this process include elimination of springback either partially or completely [5–7], reduction in anisotropy effects [8] and suppression of micro-cracks due to self healing [9]. The experimentally observed behaviour during the application of electric current is correlated to the combined effect of Joule heating and localized interaction between the electrons and the microstructure of the materials. This change in mechanical behaviour due to the application of electric current is termed as electroplasticity. In the literature, the electroplastic effect has been attributed to a combination of multiple effects such as electron-momentum transfer [10], weakening of atomic bonds due to charge imbalance near the defect sites [11] and magentoplastic effect [12] along with secondary effects such as skin and pinch effect [13]. The simplest explanation for the observed electric-assisted mechanical behaviour is the associated Joule's heating. The existence of an independent interaction between moving electrons and dislocations, in addition to the Joule heating is well established [4, 14, 15]. It has also been demonstrated that the secondary effects such as skin and pinch effect [13, 16] have negligible contribution towards the drop in flow stress observed due to electroplasticity in thin sheets. Therefore, the observed stress drop (Eq. 1) during EA forming can be represented as the superposition of thermal effect due to

✉ Jai Tiwari
me18d006@smail.iitm.ac.in

✉ Hariharan Krishnaswamy
hariharan@iitm.ac.in

1 Manufacturing Engineering Section, Department of Mechanical Engineering, Indian Institute of Technology Madras, Chennai 600036, India

2 Tribology and Combustion Division, Indian Institute Of Petroleum, Council of Scientific and Industrial Research, Dehradun 248005, India

3 Department of Metallurgical and Materials Engineering, Indian Institute of Technology Madras, Chennai 600036, India

Fig. 1 Representation of change in the mechanical behaviour during the electric-assisted forming
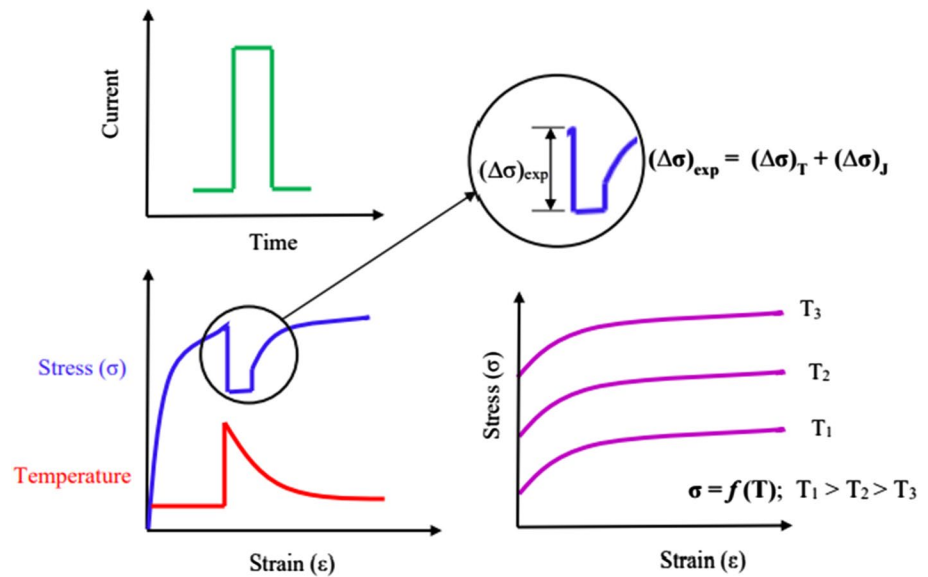
Joule's heating and the independent effect of electric current over the dislocation motion.

$$(\Delta\boldsymbol{\sigma})_{exp} = (\Delta\boldsymbol{\sigma})_T + (\Delta\boldsymbol{\sigma})_J \quad (1)$$

where $(\Delta\boldsymbol{\sigma})_{exp}$ represent the experimentally observed stress drop, the subscript 'T' and 'J' in R.H.S refers to the linearly decomposed stress components due to thermal and electroplastic effect, respectively. The superposition of the effects are represented schematically in the Fig. 1, in case of a single pulse current assisted deformation.

Consensus on the governing mechanism of this independent effect (pure electroplastic effect) is still lacking in the literature [17, 18]. The stress drop due to electroplastic effect $(\Delta\sigma_J)$ in Eq. 1 can be obtained by subtracting the contribution of the thermal effect from the overall stress drop observed during the electric-assisted deformation process. Therefore, it is critical to predict the thermal contribution accurately in order to model electroplastic effect. Modelling of electroplastic deformation has gained attention recently to underpin the mechanism of electroplasticity [19–21]. The modelling approaches should accommodate both the thermal as well as electroplastic effect in their framework [22, 23]. Since the stress drop due to Joule's heating is a function of temperature, accurate prediction of temperature history is crucial in the estimation of the thermal contribution.

In an electric-assisted forming process, the combination of electrical and mechanical loads affect the resistance of the deforming sample. To account for this change in resistance, a coefficient, ζ,[1] is used in the present analysis. A portion of

the Joule heat generated is lost to the environment and can be quantified by using an effective heat transfer coefficient (h_{eff}). Estimation of these two parameters, namely Joule heat fraction and effective heat transfer coefficient are critical in decomposing the total stress drop using Eq. 1.

Generally, these two coefficients are identified by iterative FE simulations to match the experimentally measured temperature history [5, 23]. In addition to these coefficients, the temperature history is influenced by several other thermophysical parameters such as specific heat capacity, thermal and electrical conductivity. Most of these parameters are temperature dependent that complicates the estimation of thermal coefficients through classical gradient optimization. In addition to that, EA forming involves application of multiple electrical pulses and the optimization process should simultaneously minimize the error in predicting the temperature history over multiple electrical pulses. This is a classical problem for using heuristic optimization algorithm [24–26]. The substantial growth of the multi-objective evolutionary algorithms over the years enables us to carry out such work in a more sophisticated manner [27–29]. Evolutionary algorithms can be used to avoid manual iteration [30, 31], that may yield less accurate results. A detailed review on such modelling strategies can be found in the literature [32, 33] and formulation of some of these strategies are discussed by Chakraborti [34].

In the present work, distinct optimization techniques namely, bi-objective genetic programming (BioGP) [35, 36], evolutionary neural network (EvoNN) [37] and constrained version reference vector evolutionary algorithm (cRVEA) [38, 39] have been used to identify the input thermal modelling parameters of a coupled thermal-electrical-structural analysis of an electric assisted deformation process. For this purpose, two different modes of electric assisted (EA)

[1] In the past analyses, the coefficient ζ is referred as Joule heat fraction. The same terminology is used for this coefficient in the present work, henceforth.
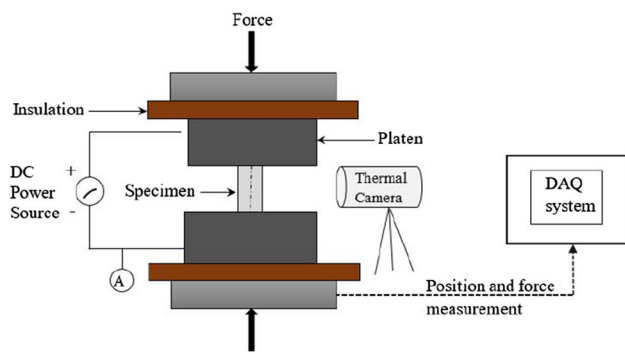
Fig. 2 Schematic diagram of an electric-assisted forming setup

Fig. 3 A representation of time-temperature profile showing the three variables (1) peak temperature (T_p), (2) background temperature (T_b) and (3) rate of cooling (θ_T) in each of the applied pulses

Table 1 Task associated with the objective functions

Objectives	Task
Peak temperature error (ϕ_1)	Minimization
Background temperature error (ϕ_2)	Minimization
Error in cooling rate (ϕ_3)	Minimization

deformation are selected in this work namely, (1) EA tension and (2) EA compression. In the subsequent sections, a brief introduction of the thermal modelling in EA deformation is presented followed by the development of training and optimization strategies. The training and optimization procedure is performed using a commercially available software, MATLAB^{TM}. The implications and necessity of the heuristic optimization is further discussed through the simulation results obtained using the optimized coefficients.

2 Methodology

Electric-assisted forming (EAF) involves simultaneous application of electric current during plastic deformation. The test set up used for conducting electric-assisted deformation experiments is schematically shown in the Fig. 2. Insulation between the platens and other machine components is provided to prevent any unintended current flow to the rest of the experimental setup. A thermal camera (non-contact type) or a pair of thermocouple wires (contact type) is employed to record the temperature history during EA deformation. A schematic representation of electric-assisted deformation behaviour is shown in the Fig. 1.

Modelling of electric-assisted deformation process requires a coupled multifield analysis to accommodate the electro-thermo-mechanical behaviour of the materials [40]. The temperature of the specimen evolves with the application of current and influences the mechanical behaviour, accordingly. Accurate prediction of temperature history is critical to decouple the thermal effect (Eq. 1) in modelling electroplasticity. The importance of accurately estimating Joule heat fraction and effective heat transfer coefficient, and the necessity of multi-objective evolutionary algorithms for optimization of error minimization have been highlighted in the previous section.

Application of electric current during the plastic deformation increases the temperature of the specimen due to Joule's heating. When the applied current is in pulsed form, heating
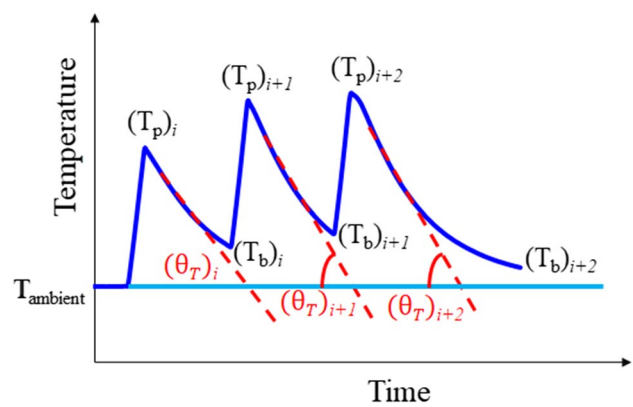
of the specimen takes place during the 'pulse on' duration. When the pulse is switched off, specimen tends to cool as a result of heat lost to the ambient environment. The pulsating time-temperature behavior of electric-assisted deformation can be defined using three parameters, (1) peak temperature (T_p), (2) background temperature (T_b) and (3) rate of cooling (θ_T) to the ambient temperature. These parameters are schematically shown in Fig. 3 in a typical time temperature profile of EA deformation. All the three parameters evolve with time during the pulse application. The subscripts i, $(i+1)$ and $(i+2)$ refer to the number of pulses applied in sequence.

A robust model should be able to predict (T_p), (T_b) and (θ_T) with reasonable accuracy in each pulse cycle. In other words, the error between the modelled and experimental results of these three parameters should be minimized simultaneously for accurate prediction of the temperature history. Using this approach, three objective functions are proposed for the optimization procedure, as shown in Eqs. 2, 3 and 4. The objective functions are essentially the normalized root mean square error (NRMSE) terms in each of the three defined parameters. The task associated with each of the objective functions is shown in the Table 1.

$$\phi_1 = \sqrt{\frac{1}{n}\Sigma_{i=0}^n \left(\frac{(T_p)_{exp} - T_p}{(T_p)_{exp}}\right)^2}, \tag{2}$$

$$\phi_2 = \sqrt{\frac{1}{n}\Sigma_{i=0}^n \left(\frac{(T_b)_{exp} - T_b}{(T_b)_{exp}}\right)^2}, \tag{3}$$

$$\phi_3 = \sqrt{\frac{1}{n}\Sigma_{i=0}^n \left(\frac{(\theta_T)_{exp} - \theta_T}{(\theta_T)_{exp}}\right)^2}, \tag{4}$$

Two sets of experimental data, EA tension and EA compression, are used to verify the accuracy of the predicted coefficients from the data driven modelling. Evolutionary approaches namely BioGP (bi-objective genetic programming) [41, 42] and EvoNN (Evolutionary Neural Network) [43, 44] are used to generate the training models for the objective functions for subsequent optimization. In EvoNN, a Pareto trade-off is established between the accuracy and complexity of the models by using the evolution process like crossover, mutation, selection at the lower part of the algorithm and linear least square method at the upper hand to converge mathematically [43, 45]. Instead of neural nets, genetic programming trees are used in BioGP model in the optimal trade-off process. As a result, multiple models are generated. The appropriate model for subsequent analysis is chosen by imposing additional criterion, such as corrected Akaike information criterion for EvoNN [46, 47] and possession of minor error model for BioGP [45]. Upon successful validation and testing of the trained models, multi-objective optimization is carried out using BioGP, EvoNN and cRVEA (constraint-based reference vector evolutionary algorithm) detailed elsewhere [36, 38, 39, 48, 49], to obtain the optimum solutions. The steps followed in the present work is shown in a flowchart (Fig. 4).

2.1 Experimental Dataset of Electric-Assisted Deformation

The data set of electric-assisted tension test is obtained from the reference [50], where the effect of pulsed current on the mechanical behaviour of AA 5052-H32 was studied. The tensile specimen dimensions were as per ASTM E8 standard except the width, which was reduced from 12.5 to 9 mm. The electric-assisted tension tests were carried out at a constant crosshead speed of 2.5 mm/min with a nominal current density of 110 A/mm². The current pulses were defined with pulse duration of 0.5 s, background current of 0 A and background time of 29.5 s. The temperature of the specimen reaches a peak value during the pulse duration and at the instant of pulse switching off (during the background time), the temperature decreases by transferring heat to the environment. The ambient temperature during the experiment is reported as 25 °C. Temperature evolution due to Joule's heating during EA deformation was measured using both a K-type thermocouple spot welded on to the sample and an infrared thermal imaging camera. The resulting temperature profile for the first 7 pulses is shown in Fig. 5a. It should be noted that the first current pulse was applied just before the movement of the crosshead.

The second data set involves pulsed current assisted compression of AA 6061-T6 alloy in the reference [51]. The compression specimen was as per ASTM E9 standard (with approximate length to diameter ratio of 1.5), with a length of 15 mm and diameter of 10.2 mm. The electric assisted experiments were performed at a constant displacement rate of 2.0 mm/min with a nominal current density of 90 A/mm². The ambient temperature during the experiment is reported as 17 °C. Temperature history during the electric-assisted compression test was measured using a FLIR-T621 infra-red thermal imaging camera. The resulting temperature profile is shown in Fig. 5b. The first current pulse was applied after the specimen deformed by 2 mm (after 60 s of start of the test).

2.2 Finite Element Modelling of EA Deformation

The electrical assisted tension and compression are simulated using finite element method to validate the temperature history obtained experimentally. Joule's law to estimate the heat transfered when passing current through a conductor is given as,

$$Q_{JH} = I^2 R_e t, \tag{5}$$

where I, R_e and t represent amount of current, effective resistance offered by the conductor and time of the current flow, respectively. As mentioned in the introduction section, the specimen is subjected to electrical and mechanical loading simultaneously during electric-assisted deformation. The combination of electrical and mechanical loads affect the resistance of the deforming sample. To account for this change in resistance, a coefficient, ζ, Joule heat fraction[2] has been used in the present analysis. This yields, $R_e = \zeta R$, where 'R' is the resistance of the material prior to the application of electric pulse. The temperature experimentally measured in the sample is due to the net effect of Joule heating and heat losses to the ambience. The thermal balance (ignoring the conversion of plastic work to heat) of such specimen under electric-assisted deformation could be represented as,

---

[2] The fraction ζ used in earlier publications did not explicitly used to scale R_e. This could possibly yield an incorrect understanding $Q_{tot} = VI = \zeta I^2 Rt + (1 - \zeta)VI$. Theoretically, such linear decomposition is not possible. It is best to describe ζ as the ratio of Q_{actual} with the ideal Q under no change in mean free path of moving dislocations.

Fig. 4 Steps followed in the present work to obtain the optimum modelling parameters
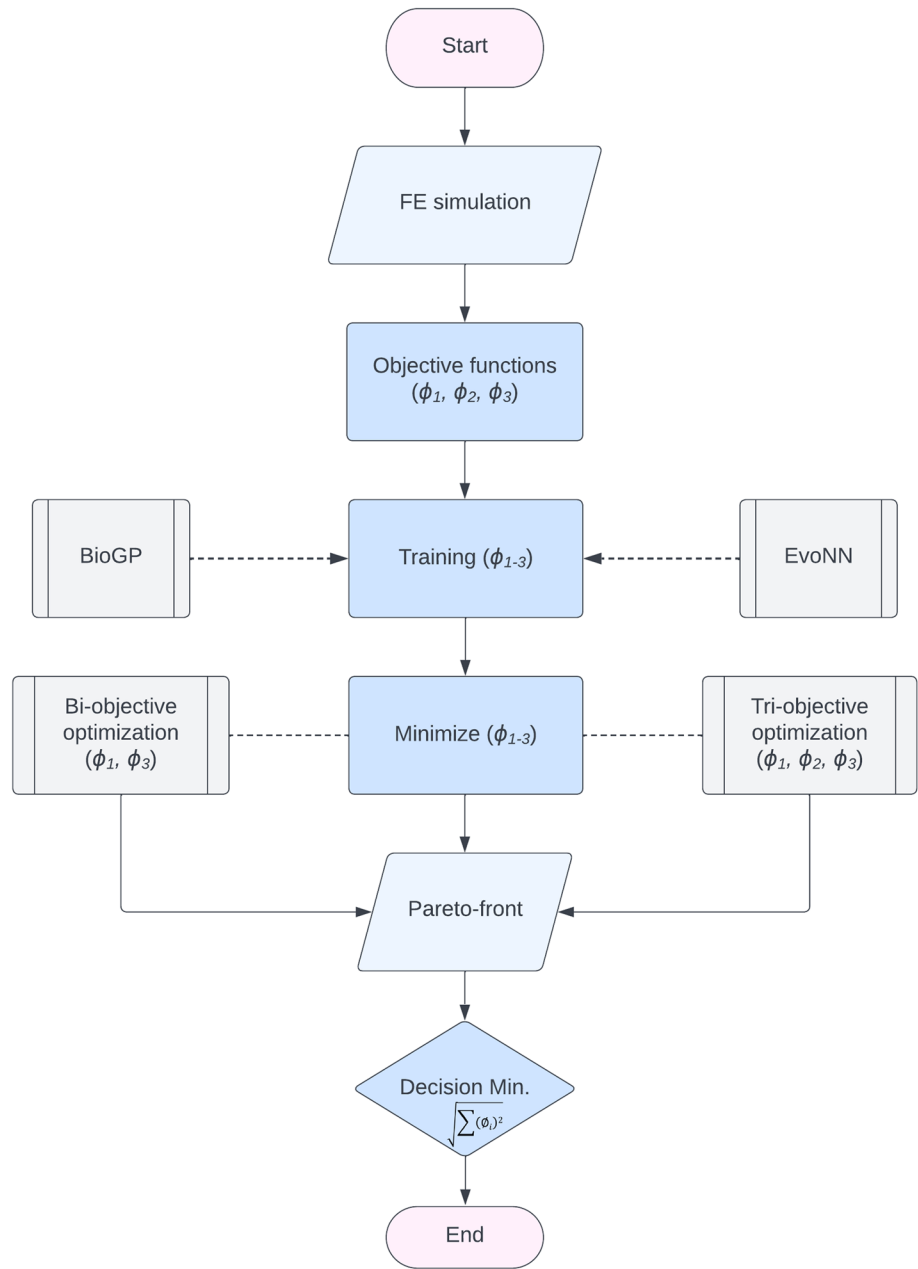

$$\Delta \dot{Q} = \dot{Q}_{JH} - \dot{Q}_{Conduction} - \dot{Q}_{Loss} \tag{6}$$

$$\rho V c_p \Delta \dot{T} = \zeta I^2 R t - k A_{cs} \nabla T - h_{eff} A_s (T - T_A) \tag{7}$$

where ρ, V, c_p and k represent the material properties such as density, volume, specific heat capacity and thermal conductivity, respectively. $\Delta \dot{T}$, A_{cs}, ∇T, h_{eff}, A_s, T and T_A represent increase in specimen temperature with time, cross section area of the specimen, temperature gradient in x, y and z directions, surface area, effective heat transfer coefficient (combining convective and radiative heat loss), instantaneous temperature of the specimen and the ambient temperature, respectively.
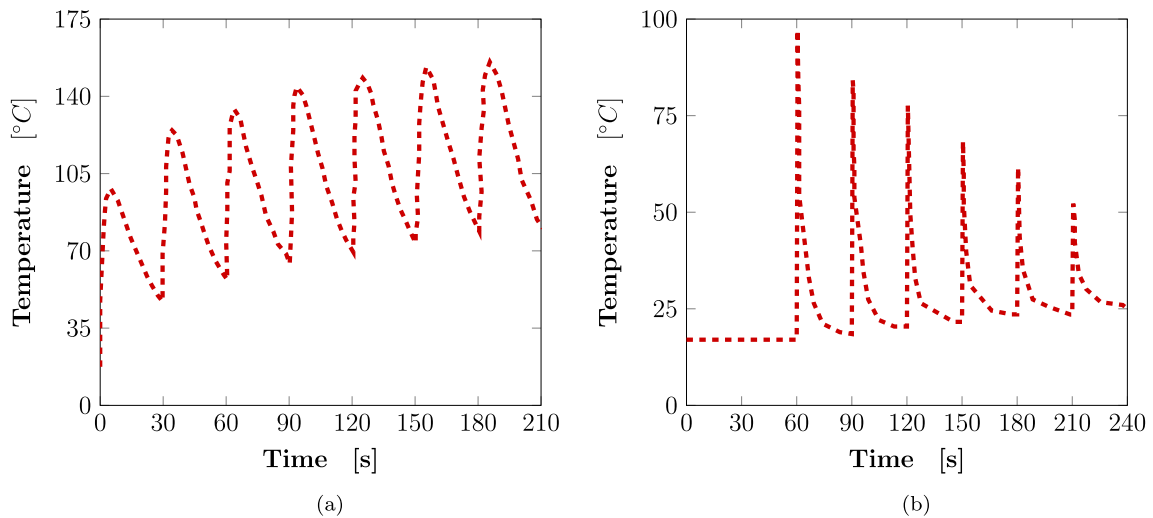
Fig. 5 Experimentally recorded time-temperature profile in case of (**a**) Electric-assisted tension [50] and (**b**) Electric-assisted compression [51]

Fig. 6 Specimen geometry modelled in the case of (**a**) electric-assisted tension (**b**) electric-assisted compression in the finite element software. The specimens are meshed with appropriate mesh sizes and the required boundary conditions are applied (Initial electrical potential [V = 0]). Heat transfer regions considered in the simulations are shown in the figures
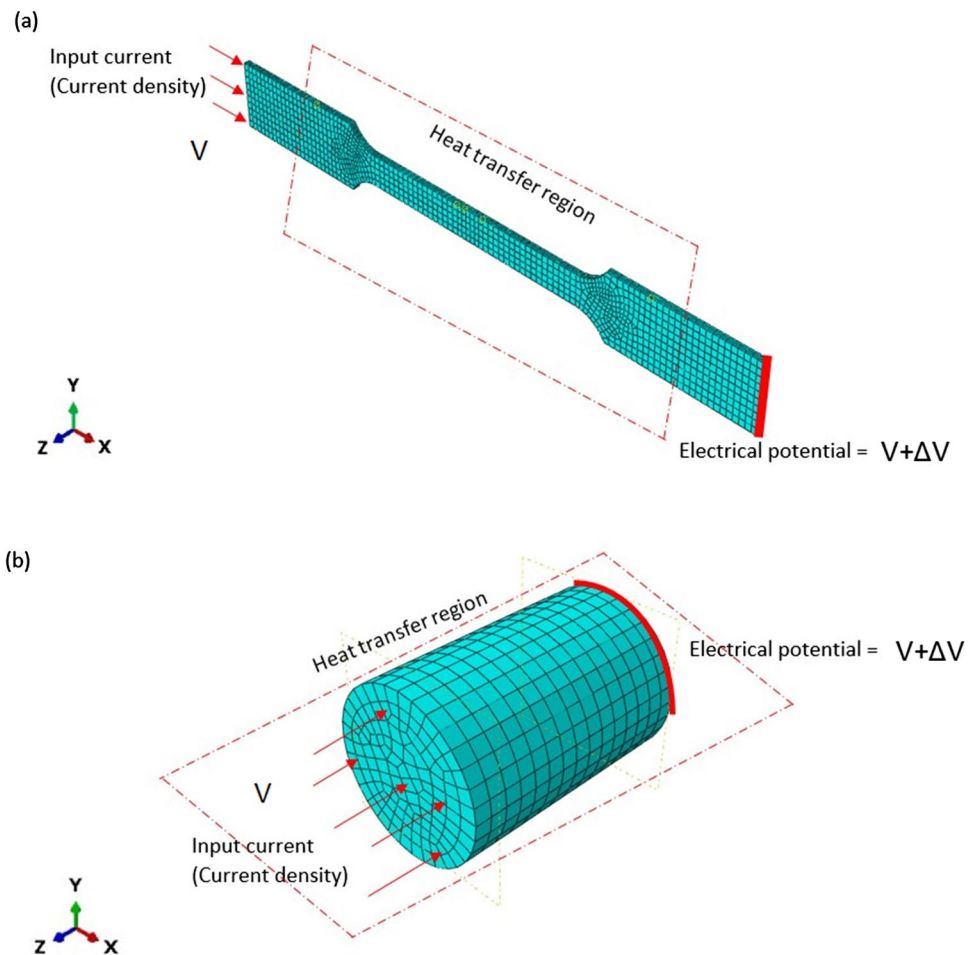
Table 2 Thermo-physical properties of AA 5052-H32 [52] and AA 6061-T6 alloy [53]

Alloy	Specific heat (J kg^{-1} K^{-1})	Thermal conductivity (W m^{-1} K^{-1})
AA 5052-H32 (tension sample)	$0.41 * T + 903$	$929 - 0.627 * T + 1.48 * 10^{-3} * T^2$
AA 6061-T6 (compression sample)	$0.1 * T + 140$	$25.2 + 0.398 * T + 7.36 * 10^{-6} * T^2$

A coupled thermal-electrical-structural analysis is performed to simulate the electric-assisted deformation in commercially available finite element software, ABAQUS®. The specimens are meshed using eight-node general purpose continuum elements, C3D8, which are compatible with the electrical load and thermo-mechanical boundary conditions. The thermal properties of the material such as specific heat and thermal conductivity are defined as temperature dependent in the analysis [52, 53]. Appropriate boundary conditions such as initial temperature field and areas for heat transfer are specified. The transient thermo-mechanical simulations are carried out on the actual time scale to predict the heat transfer from the specimens with accepted accuracy. As shown in the Fig. 6, the specimens used in the respective experiments are modelled to scale. As reported in the reference [50], a part of the specimen grip area is insulated during EA tension. Therefore, the heat transfer coefficient (h_{eff}) to accommodate heat losses was applied to the exposed area only (Fig. 6). Whereas, the film coefficient was assigned to the entire specimen (including top, bottom and side surface of the specimen) to model the heat losses in EA compression. In both the cases, electrical load was applied in form of current density on top side of the specimen to simulate the EA deformation. The bottom side of the specimen was grounded to ensure the flow of the electric current. The thermo-physical properties such as specific heat (J kg^{-1} K^{-1}) and thermal conductivity (W m^{-1} K^{-1}) of both the materials used for the present work are obtained from the reference [52] and [53], respectively (Table 2).

The definition of ζ and h_{eff} in the modelling framework is not straight forward as these two parameters are closely interrelated. Change in the magnitude of either of these coefficients would affect the evolution of the temperature profile. It should also be noted that the thermal properties of the samples are transient due to the change in specimen temperature and geometry during EA deformation process. These would affect the heat transfer from the specimen surface and in turn the time-temperature history. With multiple pulses being applied during EA deformation process, there are too many data points in the entire time-temperature profile that

Table 3 Objective function values in case of electric-assisted tension—obtained from parametric FE simulation

Input		Objective function		
ζ	h_{eff} ($\times 10^3$ W m^{-2} K^{-1})	ϕ_1	ϕ_2	ϕ_3
0.4	0.025	NA	NA	NA
0.4	0.25	NA	NA	NA
0.5	0.025	0.05264	0.12643	0.57252
0.5	0.05	0.00075	0.03884	0.22563
0.5	0.075	0.06310	0.20699	0.06250
0.5	0.1	0.00188	0.00763	0.19892
0.5	0.125	0.14864	0.16110	0.24999
0.5	0.15	0.00768	0.00448	0.31609
0.5	0.25	0.02641	0.00456	0.45030
0.55	0.0375	0.16311	0.10043	0.38751
0.55	0.125	0.08875	0.10948	0.22087
0.6	0.025	0.37365	0.02313	0.78853
0.6	0.05	0.02290	0.00281	0.37475
0.6	0.1	9.6E-07	8.8E-05	0.13216
0.6	0.15	0.00025	2.7E-05	0.27019
0.6	0.25	0.00390	0.00397	0.42920
0.65	0.0375	0.38160	0.12346	0.64194
0.65	0.075	0.16488	0.05948	0.17579
0.65	0.125	0.04229	0.08027	0.16443
0.7	0.025	1.81288	0.00331	1.00535
0.7	0.0375	0.45820	0.07660	0.73235
0.7	0.05	9.15247	0.02971	1.59795
0.7	0.1	0.00379	0.00157	0.07532
0.7	0.15	0.00049	0.01371	0.22430
0.7	0.25	0.00047	0.05177	0.40910
0.75	0.025	0.00489	0.21357	0.65917
0.75	0.125	0.15887	0.21902	0.11483
0.8	0.025	4.85971	0.00765	1.21787
0.8	0.05	0.60366	0.01045	0.66391
0.8	0.1	0.04409	0.03731	0.12438
0.8	0.15	0.00945	0.08545	0.17967
0.8	0.25	0.00433	0.29459	0.39043
0.9	0.025	4.04265	0.13838	1.43001
0.9	0.0375	0.84222	0.30031	1.08770
0.9	0.05	1.70187	0.05146	0.81135
0.9	0.1	0.21359	0.22955	0.19824
0.9	0.15	0.05628	0.68149	0.14270
0.9	0.25	0.02492	0.98264	0.36796

Table 4 Objective function values in case of electric-assisted compression—obtained from parametric FE simulation

Input		Objective function		
ζ	h_{eff} ($\times 10^3$ W m^{-2} K^{-1})	ϕ_1	ϕ_2	ϕ_3
0.4	0.1	NA	NA	NA
0.4	0.8	NA	NA	NA
0.5	0.1	NA	NA	NA
0.5	0.8	NA	NA	NA
0.6	0.10	0.01823	0.18388	0.40608
0.6	0.25	1.00634	1.02446	0.16110
0.6	0.5	0.05709	0.02344	1.29552
0.6	0.75	5.00574	5.00099	0.52273
0.6	0.8	5.00578	5.00097	0.84517
0.65	0.375	0.21997	0.17076	0.19628
0.65	0.625	0.28654	0.15221	0.18761
0.65	0.775	0.29764	0.13939	0.20280
0.7	0.1	0.10654	0.13490	0.84516
0.7	0.225	0.00289	0.02470	0.39937
0.7	0.25	0.00461	0.02415	0.43646
0.7	0.5	1.00817	1.00636	1.54050
0.7	0.8	1.01568	1.00697	0.40674
0.75	0.125	0.27358	0.31899	1.40273
0.75	0.375	0.15278	0.22010	0.24991
0.75	0.625	0.22077	0.19915	0.18326
0.75	0.775	0.23700	0.16434	0.20338
0.8	0.1	0.50081	0.16597	1.78981
0.8	0.25	1.00026	1.07284	0.63990
0.8	0.5	0.00985	0.09946	0.16568
0.8	0.75	1.00462	1.10168	0.40450
0.8	0.8	0.02084	0.10298	0.18361
0.85	0.125	0.39237	0.41372	1.61411
0.85	0.625	0.16086	0.30361	0.17977
0.85	0.775	0.09039	0.35873	0.29299
0.9	0.1	1.17632	0.37040	2.04190
0.9	0.25	1.00660	1.31900	0.70722
0.9	0.5	0.00631	0.30580	0.17616
0.9	0.75	0.01033	0.39184	0.17667
0.9	0.8	0.00824	0.48261	0.18136

Table 5 Parameters of EvoNN and BioGP for electric-assisted tension and electric-assisted compression

Processes	Electric-assisted tension		Electric-assisted compression	
Parameters	BioGP	EvoNN	BioGP	EvoNN
Hidden nodes	NA	8	NA	7
Max depth	6	NA	6	NA
Max root	8	NA	8	NA
Max rank	20	20	20	20
Kill interval	5	7	5	7
No. of preys	500	500	500	500
No. of predators	50	50	50	50
Grid size	60*60	60*60	60*60	60*60
No. of generations	20	75	20	75

Table 6 Training error in dataset of electric-assisted tension

Model	Generation	Model structure	ϕ_1	ϕ_2	ϕ_3
BioGP	20	Root=6 Depth=8	0.0729	0.0491	0.0578
		Root=8 Depth=10	0.0885	0.095	0.0542
		Root=10 Depth=10	0.09786	0.0634	0.0533
EvoNN	75	Hidden nodes=8	0.0925	0.0499	0.1227
		Hidden nodes=10	0.0916	0.0685	0.1238
		Hidden nodes=12	0.1089	0.0685	0.1367

that ζ ranges from 40-90 % for such analyses [13, 54]. The value of h_{eff} depends on various factors such as ambient temperature and the experimental conditions. The coupled electrical-thermal-structural finite element simulations were carried out with combination of the selected parameters and the obtained results were used as data input for the genetic algorithm formulation.

limits the use of iterative gradient optimization to predict the modelling parameters. Given the complexity involved in the prediction of these coefficients, as mentioned earlier, it is best to use a heuristic approach to solve this problem.

Heuristic approaches require input data over a wide range of input variable values. In the present case, the two input variables are ζ and h_{eff}. It has been shown in the literature

Table 7 Training error in dataset of electric-assisted compression

Error in data driven modelling of electric-assisted compression

Model	Generation	Model structure	ϕ_1	ϕ_2	ϕ_3
BioGP	2	Root=6 Depth=8	0.0809	0.0769	0.0840
		Root=8 Depth=10	0.0799	0.0760	0.0877
		Root=10 Depth=10	0.08151	0.0738	0.0671
EvoNN	75	Hidden nodes=7	0.0854	0.0871	0.040
		Hidden nodes=8	0.1231	0.1201	0.0525
		Hidden nodes=10	0.1061	0.116	0.0478

Table 8 RMSE between the trained dataset and the simulation results in case of electric-assisted deformation

Processes	EAT		EAC	
Objective functions	BioGP	EvoNN	BioGP	EvoNN
ϕ_1	0.09370	0.08184	0.08965	0.13520
ϕ_2	0.03018	0.03271	0.14112	0.09960
ϕ_3	0.02936	0.15642	0.05064	0.06253

numerically and are indicated as "NA" in the table. Such non convergent solutions were used to identify the lower bound of parameters in numerical iterations.

3.1 Training using BioGP and EvoNN

As a general practice in data driven modelling approaches, a fraction of the input data is used to train the models and rest is utilized to test and validate the trained models [55, 56]. Around 70 % of the data collected (Tables 3 and 4) was utilized to train both the models (BioGP and EvoNN). Ten percent of the simulation data was employed for validation. Finally, the effectiveness of the developed models was tested with the remaining 20 % data. The parameters of different algorithms are iterated to prevent either overfitting or under-fitting of the data (Table 5).

3 Results and Discussion

The dataset of the three objective functions (ϕ_1, ϕ_2 and ϕ_3) were trained using bi-objective genetic programming (BioGP) and evolutionary neural Network (EvoNN) models. The three parameters T_p, T_b and θ_T identified in each of the pulse cycles were used to calculate the objective functions (Eqs. 2, 3 and 4) and are presented in Tables 3 and 4, respectively. Few iterations in FE simulations failed to converge
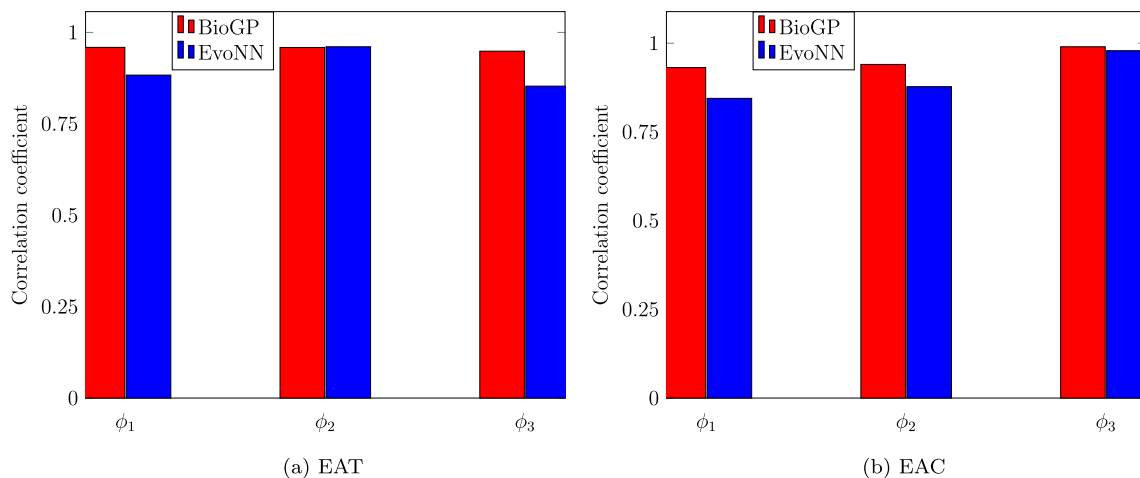

(a) EAT   (b) EAC

Fig. 7 Correlation coefficient results generated from EvoNN and BioGP in case of (**a**) Electric-assisted tension and (**b**) Electric-assisted compression

Fig. 8 The predicted values of objective functions (ϕ_1, ϕ_2 and ϕ_3) from (**a**) BioGP (left side) and (**b**) EvoNN (right side) trained models are presented with corresponding value of objective functions—obtained from FE simulation in case of electric-assisted tension
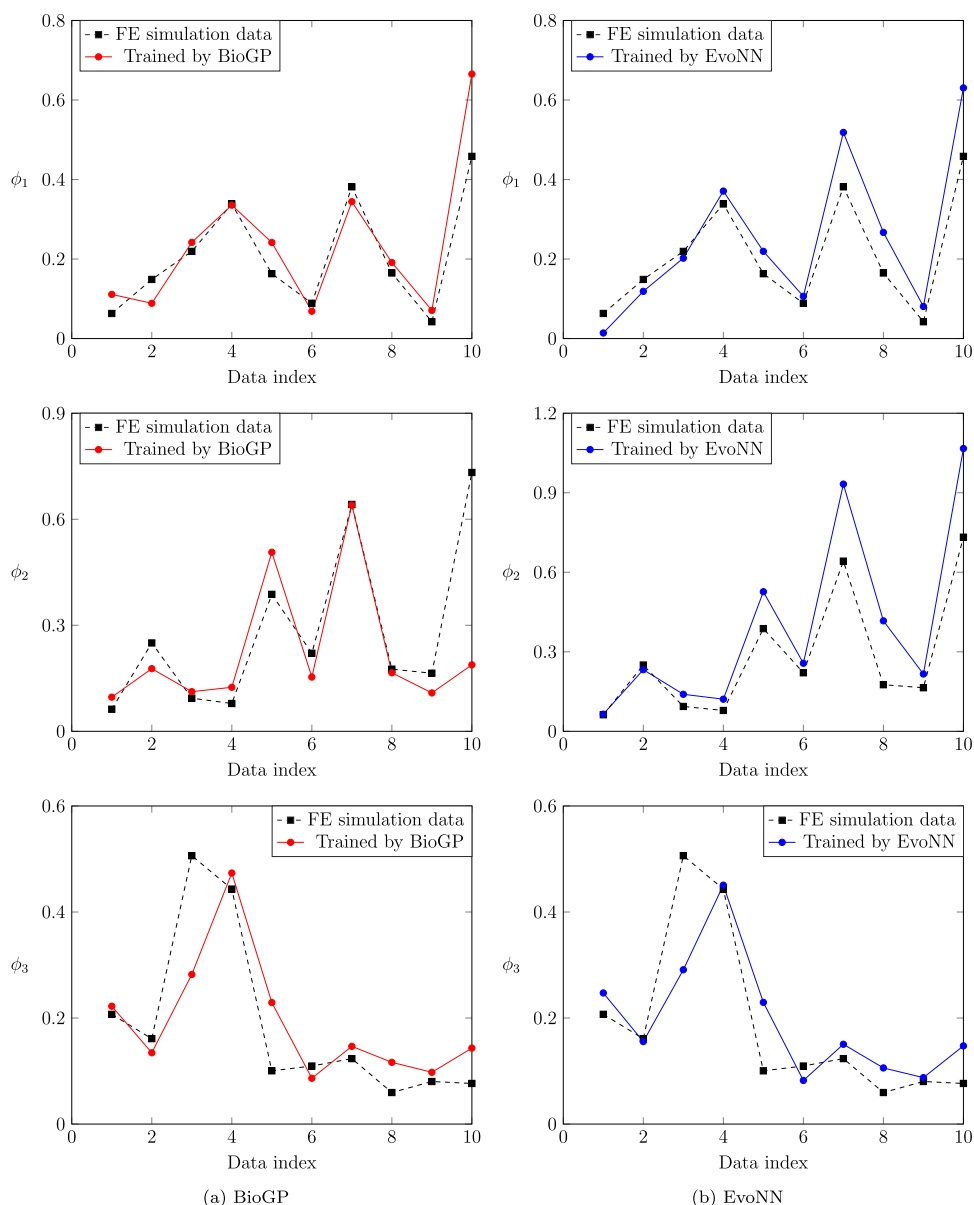

(a) BioGP

(b) EvoNN

Using the above parameters, each of the objectives, ϕ_{1-3} (Eqs. 2–4) are trained with both BioGP and EvoNN. The optimized training parameters (Table 5) are used to generate the surrogate models. The input variables for all the three objectives are ζ and h_{eff}.

As evident from the Tables 6 and 7, the error increases with the number of hidden nodes in the case of EvoNN, and root and depth in the case of BioGP model. Therefore, optimum values of these variables in the respective training models were carefully selected, which best represent the input dataset. The correlation coefficient generated from BioGP with the optimum number of depth and roots and

EvoNN with optimum number of hidden nodes are shown in the Figs. 7 (a) and (b).

The input data set has a higher degree of non-linearity and complexity. When modelled using BioGP and EvoNN, the actual trend of data could be captured with reasonable accuracy. The correlation coefficient from both the modelling strategies is more than 85 % (Fig. 7). Thus, it can be concluded that both the strategies worked in a constructive way to capture all the important trends. The predictions from both the training models are satisfactory in each of the EA deformation processes.

Fig. 9 The predicted values of objective functions (ϕ_1, ϕ_2 and ϕ_3) from (**a**) BioGP (left side) and (**b**) EvoNN (right side) trained models are presented with corresponding value of objective functions—obtained from FE simulation in case of electric-assisted compression

(a) **BioGP**   (b) **EvoNN**
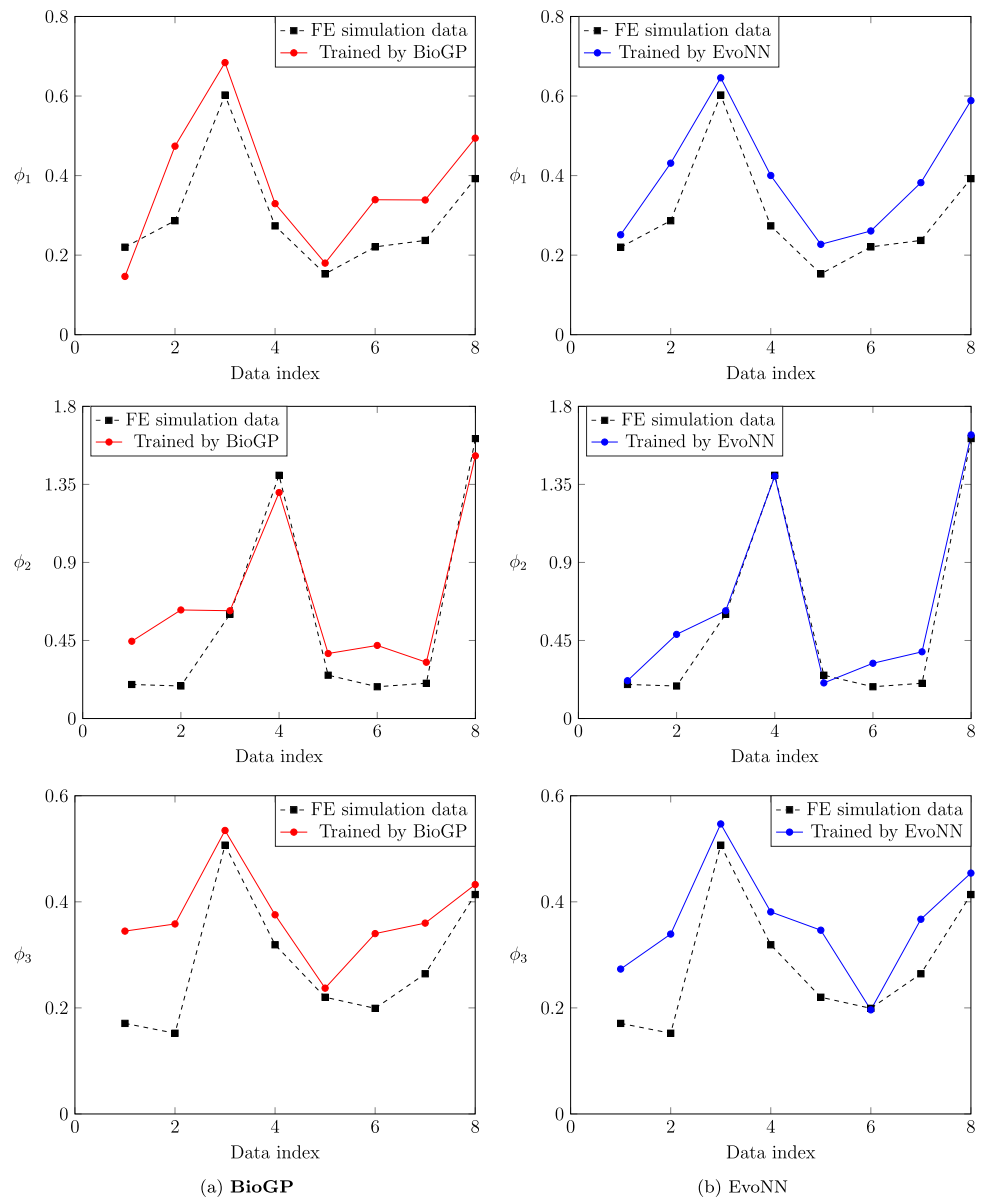
For validation purpose, the root mean square error (RMSE) between the trained data and the corresponding simulation results were calculated. The error values in both the training models are within 15 % in EA deformation modes (Table 8).

After validation, the trained models were tested with the remaining simulation results. The objectives estimated from the surrogate models were compared with the FE simulation results. It is observed (Figs. 8 and 9) that both EvoNN and BioGP capture the complexity of the objectives with reasonable accuracy.

The trained surrogate models serve as input that would be minimized simultaneously to obtain the thermal coefficients.

3.2 Optimization of the Trained Dataset

The identification of the objectives namely error in peak temperature, background temperature and cooling rate is based on the general understanding. Preliminary trials indicated that the peak temperature was sensitive to ζ and the cooling rate (θ_T) was influenced primarily by h_{eff}. Therefore, it is pertinent to establish the sufficiency condition by

Fig. 10 Pareto solutions obtained by (**a**) BioGP and (**b**) EvoNN optimization algorithms in case of electric-assisted tension, (**c**) BioGP and (**d**) EvoNN optimization algorithms in case of electric-assisted compression
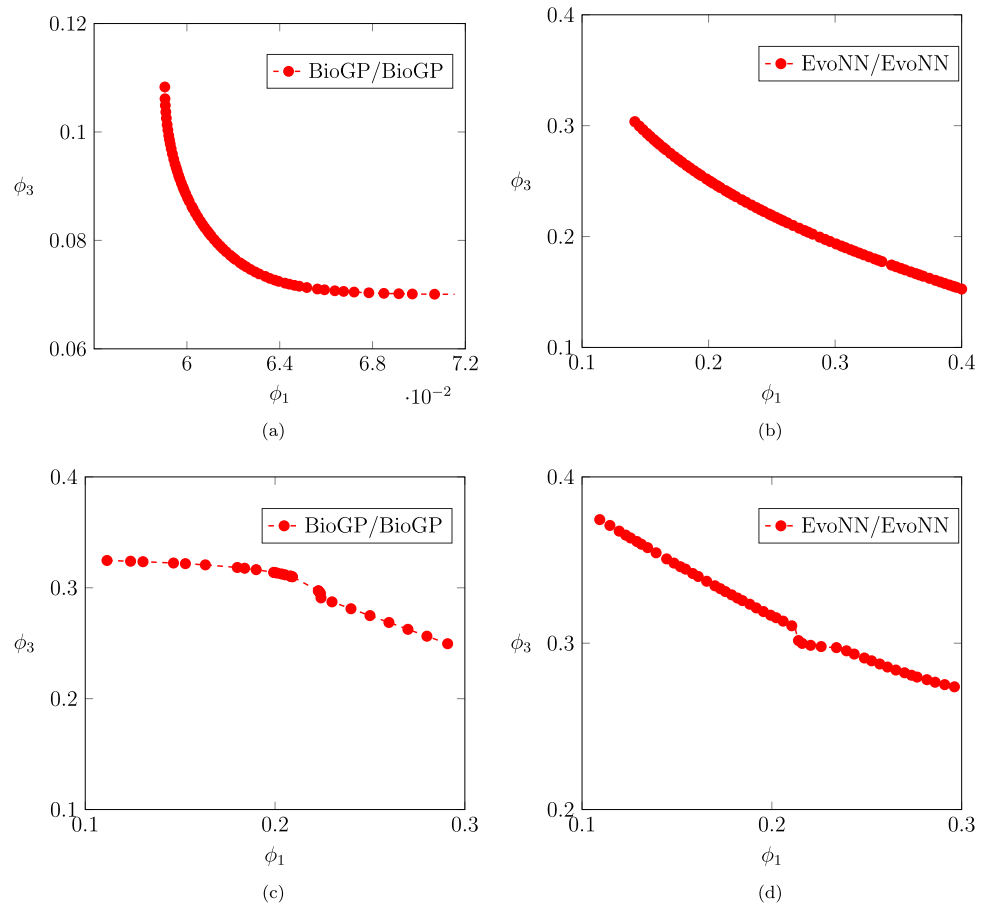
Table 9 Modelling parameters obtained using bi-objective optimization procedures

| Parameters	ζ	h_{eff}	ϕ_1	ϕ_3
Electric-assisted tension				
BioGP/BioGP	0.59	0.146	0.07863	0.21627
EvoNN/EvoNN	0.90	0.194	0.19339	0.25561
Electric-assisted compression				
BioGP/BioGP	0.65	0.54	0.30160	0.29043
EvoNN/EvoNN	0.76	0.44	0.21465	0.30062

evaluating whether bi-objective optimization using only two of the three identified objectives could give optimum solution. For this purpose, BioGP and EvoNN (bi-objective optimization processes) considering only two-objective functions i.e., peak temperature error (ϕ_1) and error in cooling rate (ϕ_3), are used for the optimization of the trained dataset.

The Pareto solutions obtained from the analysis is presented in the Fig. 10.

Each point in the Pareto front is associated with the respective error in the objectives. In such cases, a knee point, if available, is selected for the optimum solution among a group of solutions [30]. A sharp knee point is not obtained (Fig. 10) in the present analysis. Therefore, the optimum modelling parameters are identified based on the minimum distance from the origin ($\sqrt{\phi_1^2 + \phi_3^2}$) [37]. The obtained parameters along with the respective objective functions are tabulated in the Table 9. It is observed that the objective function values associated with the optimum solutions are higher than expected in each case.

The simulations of EA tension and compression carried out with the optimum values of ζ and h_{eff} and the results are presented in the Fig. 11. The error in temperature history and the $(\Delta\sigma)_T$ predicted is appreciable. It is infered that two objectives are not sufficiently accurate to predict the thermal coefficients (Fig. 11).

Fig. 11 FE simulation results of electric assisted tension test and electric assisted compression test carried out with the optimized modelling parameters obtained using (**a**), (**c**) BioGP and (**b**), (**d**) EvoNN are plotted with experimental results in respective conditions
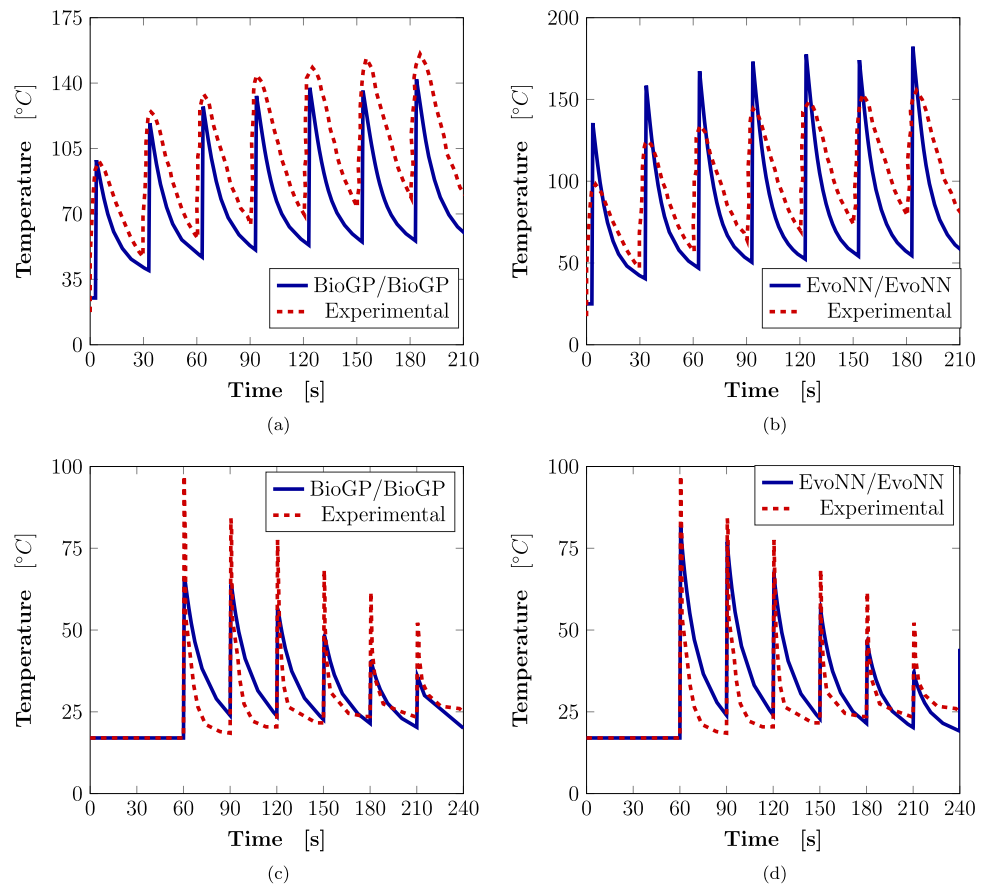
**Table 10** Modelling parameters obtained by tri-objective optimization procedures

Parameters	ζ	h_{eff}	ϕ_1	ϕ_2	ϕ_3
Electric-assisted tension					
BioGP/cRVEA	0.55	0.124	0.07198	0.26185	0.19151
EvoNN/cRVEA	0.57	0.085	0.02822	0.10053	0.17822
Electric-assisted compression					
BioGP/cRVEA	0.82	0.54	0.19128	0.3042	0.1657
EvoNN/cRVEA	0.89	0.77	0.17917	0.15617	0.21274

The optimization algorithms BioGP and EvoNN used here is limited to bi-objective optimization only. Therefore, a constraint-based reference vector evolutionary algorithm (cRVEA) is used for minimization of all the three objectives (ϕ_{1-3}). The cRVEA algorithm uses the principle of generation of reference vectors in the multi-dimensional space, assignment of an individual to the reference vector, convergence and divergence of individual by using APD (Angle penalized distance) to find out the optimum solutions in the multi-objective optimization process [38, 57]. The objectives trained by both BioGP and EvoNN models are optimized using this evolutionary algorithm, respectively. The Pareto solutions generated from the tri-objective optimization procedure in electric-assisted tension are shown in the Fig. 12. Similar plots are obtained in case of electric-assisted compression. The optimum modelling parameters using BioGP/cRVEA and EvoNN/cRVEA are identified based on the least distance from the origin, as explained above for bi-objective optimization. The obtained parameters along with the respective objective functions are tabulated in the Table 10.

The simulations are carried out with the optimized thermal coefficients of ζ and h_{eff} and the obtained results are presented along with the experimental results in the Fig. 13.

It can be observed (Tables 9 and 10) that the objective function values in case of tri-objective optimization process are lower compared to that of bi-objective optimization
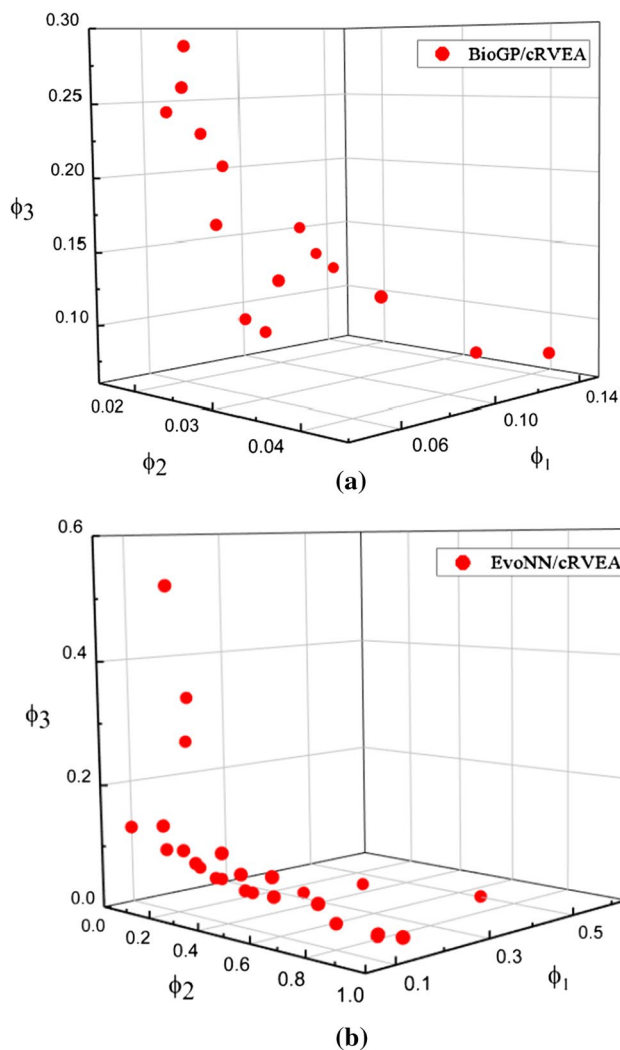
Fig. 12 Optimized solutions generated from cRVEA optimization algorithm, trained by (**a**) BioGP, (**b**) EvoNN in electric-assisted tension test

process. As a result of it, the simulations carried out using the optimized thermal coefficients obtained by tri-objective optimization process match reasonably well with the experimental results (Fig. 13). Thus, it can be concluded that the tri-objective optimization technique provides the best estimation of thermal modelling parameters of EA deformation processes.

3.3 General Trends of the Optimal Solutions

The optimal solutions obtained from tri-objective optimization are within the acceptable range as per the past analyses of the EA process [5, 13]. The optimum modelling

parameters predicted from the EvoNN/cRVEA, which produces near accurate time-temperature profile observed in the experiments, are tabulated and presented with that predicted iteratively in the reference [23, 54] in Table 11.

It is observed that the modelling parameters in both the cases indicate very good agreement with that of the reference. The time-temperature profile based on these optimum parameters predicted using GA and that obtained experimentally are compared in Figs. 13(c) and (d), showing excellent similarity between both the time-temperature profiles. This further confirms that the new methodology of identifying the thermal modelling parameters using multi-objective optimization is both accurate and reliable.
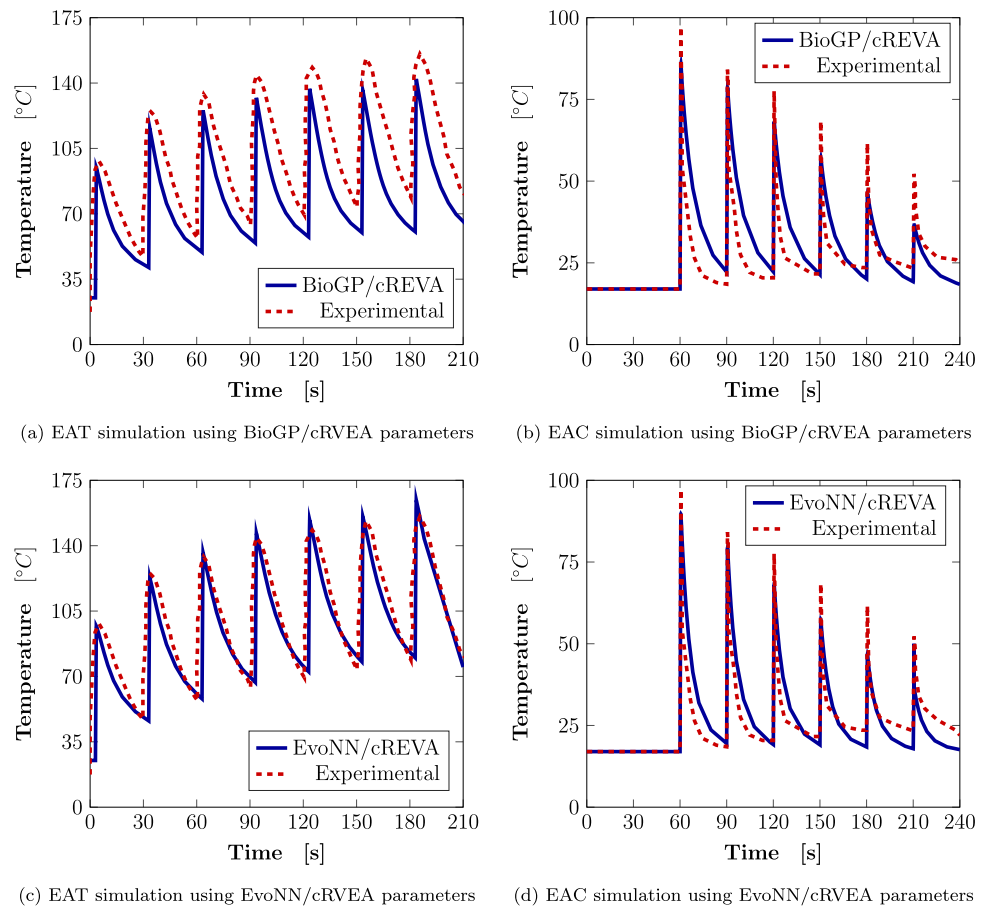
4 Conclusion

In the present work, it is shown that the evolutionary data-driven modeling and optimization approaches could be utilized to identify the thermal modelling parameters of the EA deformation process. Three objective functions are modeled using BioGP and EvoNN. In order to verify the sufficiency of the objective function in predicting ζ and h_{eff}, the trained dataset were analyzed using both bi-objective and tri-objective optimization. The conclusions from the present work are summarized below:

- Thermal modelling parameters of electric-assisted deformation as effective heat transfer coefficient and Joule heat fraction are successfully identified, using a genetic algorithm based multi-objective optimization approach.
- Unlike the traditional iterative procedures, the modelling parameters are identified where the errors between the simulated results and the experimentally obtained time-temperature profile are the least using each of the optimization procedures.
- The results indicate that when all the three error (objective) functions i.e., peak temperature, background temperature and rate of cooling are simultaneously minimized, the simulated temperature profile could be predicted within the error range of ± 5% of the experimental profile with the obtained modelling parameters.

Considering the complexities involved in such a process, usage of genetic algorithm based approaches is justified as it remove any ambiguity involved in the identification of the modelling parameters. The proposed methodology provides best estimation of the parameters in both modes of electric-assisted deformation, clearly highlighting the benefits of using this novel approach.

Fig. 13 FE simulation results of electric assisted tension test and electric assisted compression test carried out with (**a**), (**b**) BioGP/cRVEA and (**c**), (**d**) EvoNN/cRVEA optimized modelling parameters are plotted with respective experimental results, respectively

(a) EAT simulation using BioGP/cRVEA parameters

(b) EAC simulation using BioGP/cRVEA parameters

(c) EAT simulation using EvoNN/cRVEA parameters

(d) EAC simulation using EvoNN/cRVEA parameters

Table 11 Comparison of modelling parameters obtained by genetic algorithm and reference

Processes	Electric-assisted tension		Electric-assisted compression	
Parameters	ζ	h_{eff}	ζ	h_{eff}
EvoNN/cRVEA	0.57	0.085	0.89	0.77
From reference	0.60	0.10	0.90	0.765

Declarations

Conflict of interest The authors declare that they have no known competing financial interests or personal relationships that could have appeared to influence the work reported in this paper.

References

1. R. Fan, J. Magargee, P. Hu, J. Cao, Influence of grain size and grain boundaries on the thermal and mechanical behavior of 70/30 brass under electrically-assisted deformation. Mater. Sci. Eng. A **574**, 218–225 (2013)

2. J.-H. Roh, J.-J. Seo, S.-T. Hong, M.-J. Kim, H.N. Han, J.T. Roth, The mechanical behavior of 5052–H32 aluminum alloys under a pulsed electric current. Int. J. Plast. **58**, 84–99 (2014)

3. J.T. Roth, I. Loker, D. Mauck, M. Warner, S.F. Golovashchenko, A. Krause, Enhanced formability of 5754 aluminum sheet metal using electric pulsing, in *Transactions of the North American-manufacturing research institution of SME 2008*. Paper Presented at NAMRC 36. Monterrey, 20-23 May 2008, vol. 36 (SEM, Southfield, 2008), pp. 405–412

4. W. Cao, A. Sprecher, H. Conrad, Measurement of the electroplastic effect in nb. J. Phys. E Sci. Instrum. **22**(12), 1026 (1989)

5. J. Lee, H.J. Bong, Y.-S. Lee, D. Kim, M.-G. Lee, Pulsed electric current v-bending springback of AZ31B magnesium alloy sheets. Metall. Mater. Trans. A **50**(6), 2720–2731 (2019)

6. N. Mohammadtabar, M. Bakhshi-Jooybari, H. Gorji, R. Jamaati, J.A. Szpunar, Effect of electric current pulse type on springback, microstructure, texture, and mechanical properties during v-bending of AA2024 aluminum alloy. J. Manuf. Sci. Eng. **143**(1), 011004 (2021)

7. C. Li, Z. Xu, L. Peng, X. Lai, An electric-pulse-assisted stamping process towards springback suppression and precision fabrication of micro channels. Int. J. Mech. Sci. **218**, 107081 (2022)

8. A.D. Pleta, M.C. Krugh, C. Nikhare, J.T. Roth, An investigation of anisotropic behavior on 5083 aluminum alloy using electric current, in *Proceedings of the ASME 2013 International Manufacturing Science and Engineering Conference collocated with the 41st North American Manufacturing Research Conference. Volume 1: Processing*, Madison, 10–14 June 2013 (ASME, 2013), p. V001T01A018

9. K.V. Kukudzhanov, Modeling of self-healing of microcracks in the process of longitudinal electroplastic rolling. J. Phys. Conf. Ser. **2231**, 012022 (2022)

10. H. Conrad, Electroplasticity in metals and ceramics. Mater. Sci. Eng. A **287**(2), 276–287 (2000)

11. M.-J. Kim, S. Yoon, S. Park, H.-J. Jeong, J.-W. Park, K. Kim, J. Jo, T. Heo, S.-T. Hong, S.H. Cho et al., Elucidating the origin of electroplasticity in metallic materials. Appl. Mater. Today **21**, 100874 (2020)

12. M. Molotskii, V. Fleurov, Magnetic effects in electroplasticity of metals. Phys. Rev. B **52**(22), 15829 (1995)

13. K. Okazaki, M. Kagawa, H. Conrad, An evaluation of the contributions of skin, pinch and heating effects to the electroplastic effect in titatnium. Mater. Sci. Eng. **45**(2), 109–116 (1980)

14. A. Lahiri, P. Shanthraj, F. Roters, Understanding the mechanisms of electroplasticity from a crystal plasticity perspective. Modell. Simul. Mater. Sci. Eng. **27**(8), 085006 (2019)

15. X. Li, Z. Xu, P. Guo, L. Peng, X. Lai, Electroplasticity mechanism study based on dislocation behavior of Al6061 in tensile process. J. Alloys Compd. **910**, 164890 (2022)

16. J. Tiwari, P. Pratheesh, O. Bembalge, H. Krishnaswamy, M. Amirthalingam, S. Panigrahi, Microstructure dependent electroplastic effect in AA 6063 alloy and its nanocomposites. J. Mater. Res. Technol. **12**, 2185–2204 (2021)

17. S. Izadpanah, X. Cao, D. An, X. Li, J. Chen, One step forward to electrically-assisted forming mechanisms and computer simulation: A review. Adv. Eng. Mater. (2022). https://doi.org/10.1002/adem.202200425

18. N.K. Dimitrov, Y. Liu, M.F. Horstemeyer, Electroplasticity: a review of mechanisms in electro-mechanical coupling of ductile metals. Mech. Adv. Mater. Struct. **29**, 705–716 (2020)

19. M.-J. Kim, H.-J. Jeong, J.-W. Park, S.-T. Hong, H.N. Han, Modified johnson-cook model incorporated with electroplasticity for uniaxial tension under a pulsed electric current. Met. Mater. Int. **24**(1), 42–50 (2018)

20. X. Wang, J. Xu, Z. Jiang, W.-L. Zhu, D. Shan, B. Guo, J. Cao, Size effects on flow stress behavior during electrically-assisted micro-tension in a magnesium alloy AZ31. Mater. Sci. Eng. A **659**, 215–224 (2016)

21. Y. Liu, M. Wan, B. Meng, Multiscale modeling of coupling mechanisms in electrically assisted deformation of ultrathin sheets: an example on a nickel-based superalloy. Int. J. Mach. Tools Manuf. **162**, 103689 (2021)

22. H. Krishnaswamy, M.J. Kim, S.-T. Hong, D. Kim, J.-H. Song, M.-G. Lee, H.N. Han, Electroplastic behaviour in an aluminium alloy and dislocation density based modelling. Mater. Des. **124**, 131–142 (2017)

23. J. Tiwari, V. Balaji, H. Krishnaswamy, M. Amirthalingam, Dislocation density based modelling of electrically assisted deformation process by finite element approach. Int. J. Mech. Sci. **227**, 107433 (2022)

24. R. Dewri, N. Chakraborti, Simulating recrystallization through cellular automata and genetic algorithms. Modell. Simul. Mater. Sci. Eng. **13**(2), 173 (2004)

25. D. Hong, S. Kwon, C. Yim, Exploration of machine learning to predict hot ductility of cast steel from chemical composition and thermal conditions. Metals Mater. Int. **27**(2), 298–305 (2021)

26. D. Mohanty, A. Chandra, N. Chakraborti, Genetic algorithms based multi-objective optimization of an iron making rotary kiln. Comput. Mater. Sci. **45**(1), 181–188 (2009)

27. C.A.C. Coello, G.B. Lamont, D.A. Van Veldhuizen, *Evolutionary Algorithms for Solving Multi-Objective Problems* (Springer, New York, 2007)

28. A. Konak, D.W. Coit, A.E. Smith, Multi-objective optimization using genetic algorithms: a tutorial. Reliab. Eng. Syst. Saf. **91**(9), 992–1007 (2006)

29. P. Nagraj, P. Sadasivam, G. Saravana, G. Kumar, M. Amirthalingam, Data-driven modelling of complex current-voltage waveform controlled gas metal arc-wire ded processes. Met. Mater. Int. (2022). https://doi.org/10.1007/s12540-022-01285-7

30. K. Hariharan, N. Chakraborti, F. Barlat, M.-G. Lee, A novel multi-objective genetic algorithms-based calculation of hill's coefficients. Metall. Mater. Trans. A **45**(6), 2704–2707 (2014)

31. U. Khandey, S. Ghosh, K. Hariharan, Machining parameters optimization for satisfying the multiple objectives in machining of mmcs. Mater. Manuf. Process. **32**(10), 1082–1093 (2017)

32. N. Chakraborti, in *Informatics for Materials Science and Engineering: Data-driven Discovery for Accelerated Experimentation and Application*, ed. by K. Rajan (Butterworth-Heinemann, Oxford, 2013), pp. 71–95

33. N. Chakraborti, in *Applications of Metaheuristics in Process Engineering*, ed. by J. Valadi, P. Siarry (Springer, Cham, 2014), pp. 89–122

34. N. Chakraborti, *Data-Driven Evolutionary Modeling in Materials Technology* (CRC Press, Boca Raton, 2022)

35. A. Agarwal, F. Pettersson, A. Singh, C.S. Kong, H. Saxén, K. Rajan, S. Iwata, N. Chakraborti, Identification and optimization of ab2 phases using principal component analysis, evolutionary neural nets, and multiobjective genetic algorithms. Mater. Manuf. Process. **24**(3), 274–281 (2009)

36. B.K. Giri, J. Hakanen, K. Miettinen, N. Chakraborti, Genetic programming through bi-objective genetic algorithms with a study of a simulated moving bed process involving multiple objectives. Appl. Soft Comput. **13**(5), 2613–2623 (2013)

37. K. Hariharan, N.-T. Nguyen, N. Chakraborti, F. Barlat, M.-G. Lee, Determination of anisotropic yield coefficients by a data-driven multiobjective evolutionary and genetic algorithm. Mater. Manuf. Proces. **30**(4), 403–413 (2015)

38. B.K. Mahanta, N. Chakraborti, Tri-objective optimization of noisy dataset in blast furnace iron-making process using evolutionary algorithms. Mater. Manuf. Process. **35**(6), 677–686 (2020)

39. S. Roy, A. Dutta, N. Chakraborti, A novel method of determining interatomic potential for Al and Al-Li alloys and studying strength of Al-Al3Li interphase using evolutionary algorithms. Comput. Mater. Sci. **190**, 110258 (2021)

40. J. Tiwari, H. Krishnaswamy, M. Amirthalingam, Modelling Transient Mechanical Behavior of Aluminum Alloy During Electric-Assisted Forming, in *NUMISHEET 2022: Proceedings of the 12th International Conference and Workshop on Numerical Simulation of 3D Sheet Metal Forming Processes*, ed. by K. Inal, J. Levesque, M. Worswick, C. Butcher. Toronto, 10–14 July 2022 (Springer, Cham, 2022), pp. 105–113

41. S. Chowdhury, N. Chakraborti, P.K. Sen, Energy optimization studies for integrated steel plant employing diverse steel-making route: models and evolutionary algorithms-based approach. Miner. Process. Extr. Metall. Rev. **42**(6), 355–366 (2021)

42. C.-H. Wu, D.-Y. Yang, Bi-objective optimization of a queueing model with two-phase heterogeneous service. Comput. Operat. Res. **130**, 105230 (2021)

43. F. Pettersson, N. Chakraborti, H. Saxén, A genetic algorithms based multi-objective neural net applied to noisy blast furnace data. Appl. Soft Comput. **7**(1), 387–397 (2007)

44. D.N. Mondal, K. Sarangi, F. Pettersson, P.K. Sen, H. Saxén, N. Chakraborti, Cu–Zn separation by supported liquid membrane analyzed through multi-objective genetic algorithms. Hydrometallurgy **107**(3–4), 112–123 (2011)

45. N. Chakraborti, in *Computational Approaches to Materials Design: Theoretical and Practical Aspects*, ed. by S. Datta, J.P. Davim (IGI Global, Hershey, 2016), pp. 346–368

46. K.P. Burnham, D.R. Anderson, Multimodel inference: understanding AIC and BIC in model selection. Sociol. Methods Res. **33**(2), 261–304 (2004)

47. B. Bhattacharya, G.D. Kumar, A. Agarwal, Ş Erkoç, A. Singh, N. Chakraborti, Analyzing Fe-Zn system using molecular dynamics, evolutionary neural nets and multi-objective genetic algorithms. Comput. Mater. Sci. **46**(4), 821–827 (2009)

48. K. Deb, in *Multi-objective Evolutionary Optimisation for Product Design and Manufacturing*, ed. by L. Wang, A.H.C. Ng, K. Deb (Springer, London, 2011), pp. 3–34

49. R. Jha, P.K. Sen, N. Chakraborti, Multi-objective genetic algorithms and genetic programming models for minimizing input carbon rates in a blast furnace compared with a conventional analytic approach. Steel Res. Int. **85**(2), 219–232 (2014)

50. M.-J. Kim, K. Lee, K.H. Oh, I.-S. Choi, H.-H. Yu, S.-T. Hong, H.N. Han, Electric current-induced annealing during uniaxial tension of aluminum alloy. Scripta Materialia **75**, 58–61 (2014)

51. S.-T. Hong, Y.-H. Jeong, M.N. Chowdhury, D.-M. Chun, M.-J. Kim, H.N. Han, Feasibility of electrically assisted progressive forging of aluminum 6061-T6 alloy. CIRP Ann. **64**(1), 277–280 (2015)

52. TALAT Lectures 2502: Material Aspects of Fire Design, prepared by S. Lundberg, Hydro Aluminium Structures, Karmoy (European Aluminium Association, Brussels, 1994)

53. Z. Sun, C. Wu, S. Kumar, Determination of heat generation by correlating the interfacial friction stress with temperature in friction stir welding. J. Manuf. Process. **31**, 801–811 (2018)

54. K. Hariharan, M.-G. Lee, M.-J. Kim, H.N. Han, D. Kim, S. Choi, Decoupling thermal and electrical effect in an electrically assisted uniaxial tensile test using finite element analysis. Metall. Mater. Trans. A **46**(7), 3043–3051 (2015)

55. D. Srinivasu, N.R. Babu, A neuro-genetic approach for selection of process parameters in abrasive waterjet cutting considering variation in diameter of focusing nozzle. Appl. Soft Comput. **8**(1), 809–819 (2008)

56. S. Chakraborty, P.P. Chattopadhyay, S.K. Ghosh, S. Datta, Incorporation of prior knowledge in neural network model for continuous cooling of steel using genetic algorithm. Appl. Soft Comput. **58**, 297–306 (2017)

57. B.K. Mahanta, R. Jha, N. Chakraborti, in *Machine Learning in Industry*, ed. by S. Datta, J. Paulo Davim (Springer, Cham, 2022), pp. 47–81